S. R. Iovanovici

Empirical Evaluation of Noble Metal Extraction in Molten Salt Reactors by Helium Bubbling

Through the use of Simulants in an Experimental Setup

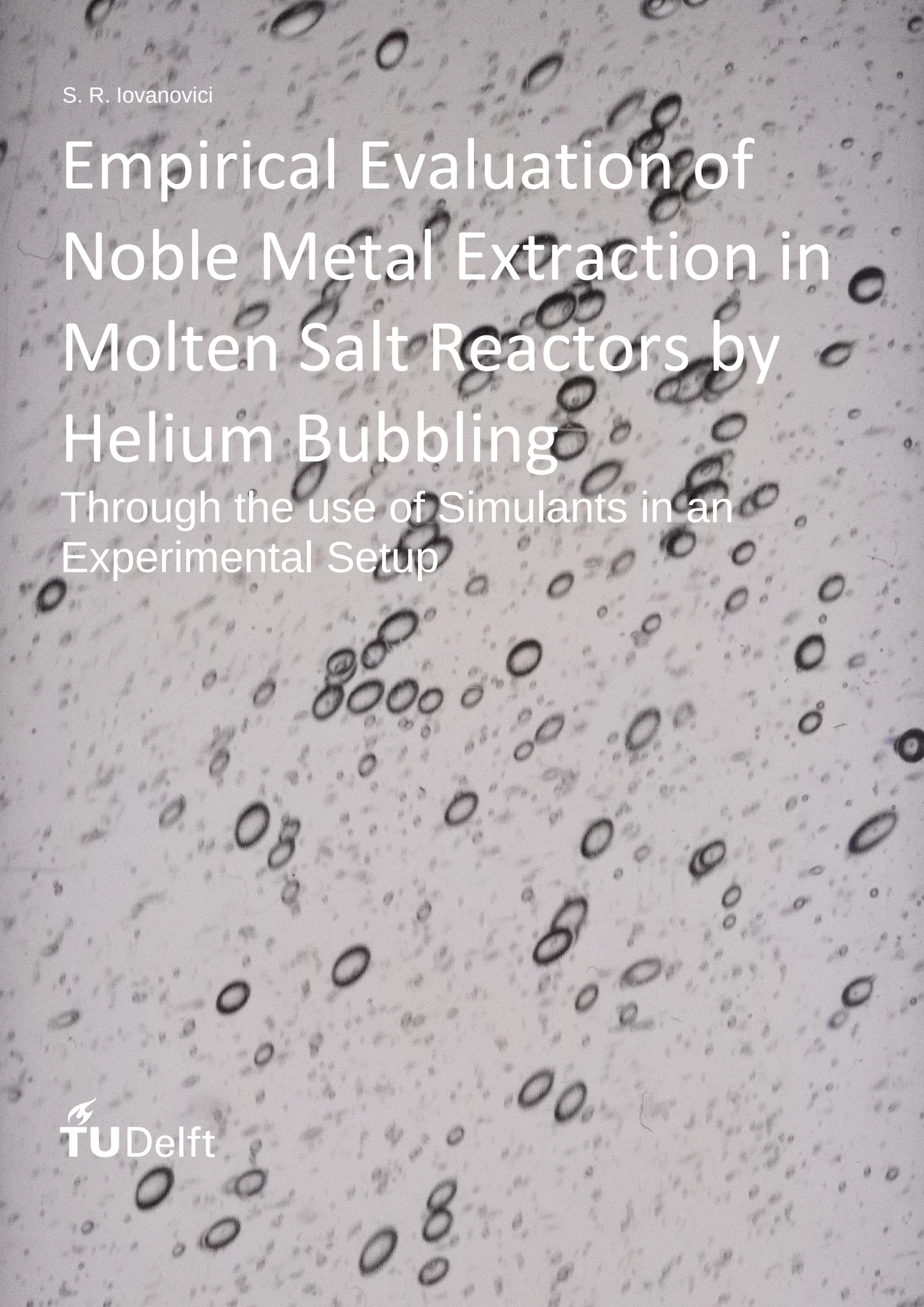

TU Delft

Empirical Evaluation of Noble Metal Extraction in Molten Salt Reactors by Helium Bubbling

Through the use of Simulants in an Experimental Setup

By

S. R. Iovanovici

in partial fulfilment of the requirements for the degree of

Bachelor of Science
in Applied Physics

at the Delft University of Technology,
to be defended publicly on Tuesday February 12, 2019 at 10:00 AM.

Supervisor:	Dr. E. Capelli	
Thesis committee:	Dr. E. Capelli,	TU Delft
	Dr. A. L. Smith,	TU Delft
	Prof. dr. ir. J. L. Kloosterman,	TU Delft

TU Delft

Contents

Abstract

In the last decades, concerns over the growing global energy demand and the current climate goals have led to the formation of an international collaboration for the research and development of new and sustainable nuclear energy systems. One of the most promising concepts that has been selected from over a hundred applications, is the molten salt reactor (MSR), a nuclear energy system design that has been developed at Oak Ridge National Laboratory. The most distinctive feature of the MSR is the use of molten salt in which fissile materials are dissolved in liquid salt. The MSR, as a concept, features a number of beneficial properties such as: an inherently safe design due to the highly negative feedback coefficients, low operating pressure fail-safe draining systems, as well as sustainability through its breeding capabilities within the thorium-uranium cycle. However, while the molten salt reactor delivers promising features, research and development still needs to be done to improve various aspects of the design before commercial deployment can be made viable.

In particular, one of the research field concerning molten salt reactors is the study of the on-line processing of molten salt. While an extraction technique known as helium bubbling has been developed in the past for the extraction of gaseous fission products from the molten salt, recent studies have been conducted to access the viability of using the same technique to extract noble metals through a process called flotation. Noble metal extraction in molten salt reactors is desired as the build-up of particles on various reactor components could possibly limit their functionality or cause damage through the accumulation of decay heat.

In this study, a review of the flotation theory is laid out and the effect of a number of flotation parameters on the mean bubble size, the gas holdup and the fine particle flotation extraction efficiency is explored through the use of an experimental setup. In this experimental setup, a Venturi type bubble generator and a flotation column are used to simulate a bypass loop of a molten salt reactor through the use of simulant particles and a simulant fluid. To this end, a water-glycerol (66-33 vol%) mixture with a kinematic viscosity similar to molten salt and molybdenum particles of varying sizes are used the simulate the flow characteristics of a molten salt reactor.

Image analysis is used to study the effect of gas- and fluid flow rates on the mean bubble size and to study the effect of the gas flow rate on the mean gas holdup. The results of this study have shown that the mean bubble size produced by a Venturi type bubble generator is only marginally influenced by the gas flow rate, while an increase in fluid flow rate is shown to correlate to a decrease in mean bubble size. Furthermore, a linear correlation between the gas flow rate and the gas holdup volume is observed.

A series of particle extraction measurements are performed to observe the effect of the gas- and fluid flow rates on the extraction efficiency of fine particles for three different particles sizes. The experiments have shown that an increase in both fluid flow rate and gas flow rate result in higher recoveries for 3-7 micron particles and 1-2 micron particles, while a decrease in particle size has been shown to negatively impact the flotation process efficiency. Finally, the total extraction of the nanoparticles has been observed to be 5.63% for a gas flow rate of 50 cm^3/min and a fluid flow rate of 0.50 l/s.

Acknowledgements

The author wishes to express his gratitude to Dr. E. Capelli for her continuous involvement as supervisor throughout the entire research project and to Prof. dr. ig. J. L. Kloosterman for his involvements in establishing contact with the appropriate project supervisors.

1. Introduction

In the wake of nuclear accidents, such as Chernobyl, Three Mile Island and the more recent Fukushima Daiichi accident, concerns regarding general safety surrounding nuclear energy, nuclear proliferation and the risk of nuclear terrorism have increased significantly and have led countries to reconsider the use of nuclear energy in their energy policies (International Energy Agency; Nuclear Energy Agency, 2015). These socio-political reasons alongside potential financing challenges (Orayeva, 2018), have resulted in the phasing out of nuclear energy systems in a number of countries and have also resulted in the preference for increasing the life time of current reactors to the decommissioning of old reactors and the construction of new ones (International Energy Agency; Nuclear Energy Agency, 2015). Overall, the number of new nuclear reactor constructions appear to have been relatively stagnant during the past thirty years (Figure 1).

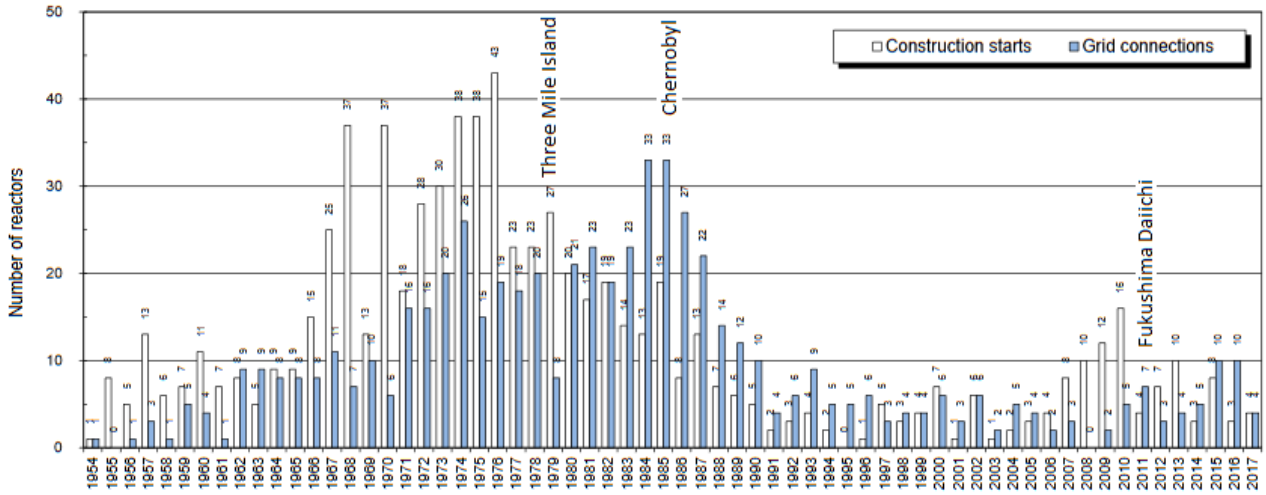

Figure 1. The number of reactor construction starts and grid connections per year (International Atomic Energy Agency , 2018).

Despite current concerns regarding the currently used second and third generation nuclear energy systems alongside other challenges in the nuclear power sector, a significant number of countries have started to show a renewed interest in starting new nuclear power programs and expanding existing ones (International Energy Agency; Nuclear Energy Agency, 2015). More than forty developing countries have shown interest in starting a nuclear program (Kaplan, 2008), and other countries such as China, Russia, India and Korea are projected to expand their nuclear power capacity significantly in the following thirty years (International Energy Agency; Nuclear Energy Agency, 2015). Moreover, current projections may indicate the significant relevance that nuclear energy will play in meeting the world energy demand and for reaching current climate goals set for 2050.

With these future prospects in mind, research and development has already started in the attempt to address existing concerns and to use the experience gained from the development and construction of second and third generation reactors to develop promising fourth generation reactor systems, which are expected to reach commercial viability near or after 2030, when many nuclear power plants in the world will be at or near the end of their operating licenses (Nuclear Energy Advisory Committee; Generation IV International Forum, 2002).

1.1 Generation IV Reactors

The collaborative international endeavour known as the Generation IV International Forum (GIF) was officially formed in 2001 in a joint effort for the research and development of fourth-generation nuclear energy systems as to work towards new sustainable sources of energy (Generation IV International Forum, 2018). The original goals set in the 2002 Roadmap and the 2014 Roadmap Update are summarized as followed (Nuclear Energy Advisory Committee; Generation IV International Forum, 2002):

- Sustainability: sustainable energy generation and the promotion of long-term availability of nuclear fuel, minimization of nuclear waste and the reduction of the long-term stewardship burden.
- Safety and reliability: excel in safety and reliability, a very low likelihood and degree of reactor core damage and the elimination for the need of offsite emergency response.
- Economics: having a life cycle cost advantage over other energy sources and having a level of financial risk comparable to other energy projects.
- Proliferation resistance and physical protection: be a very unattractive route for diversion or theft of weapon-usable materials and provide increased physical protection against acts of terrorism.

Additionally, another set of research goals were introduced after the Fukushima Daiichi accident, which relate in particular to (Nuclear Energy Agency; Generation IV International Forum, 2014):

- The use of non-water coolants in most gen-IV designs,
- higher operating temperatures,
- higher reactor power density.

Candidate concepts were discussed until a consensus was reached on the six most promising nuclear energy systems, these systems are summarized in Table 1.

Table 1. Summary of the selected six nuclear systems (Generation IV International Forum, 2018).

System	*Neutron spectrum*	*Coolant*	*Outlet Temperature °C*	*Fuel cycle*	*Size (MW_e)*
VHTR (Very-high-temperature reactor)	Thermal	Helium	900-1000	Open	250-300
SFR (Sodium-cooled fast reactor)	Fast	Sodium	500-550	Closed	50-150 300-1500 600-1500
SCWR (Supercritical-water-cooled reactor)	Thermal/fast	Water	510-625	Open/closed	300-700 1000-1500
GFR (Gas-cooled fast reactor)	Fast	Helium	850	Closed	1 200
LFR (Lead-cooled fast reactor)	Fast	Lead	480-570	Closed	20-180 300-1200 600-1000
MSR (Molten salt reactor)	Thermal/fast	Fluoride salts	700-800	Closed	1000

1.2 The Molten Salt Reactor (MSR)

The MSR (Figure 2) is a distinct class of high temperature reactor systems in which the traditional solid fuel is replaced by a circulating salt in which fissile and fertile materials are dissolved. The salts used in MSRs, usually consisting of a mixture of lithium- and beryllium-fluoride, are highly suited for use in nuclear reactors as they can act as a nuclear reaction medium, a heat transfer medium and as a chemical processing medium simultaneously (Furukawa, et al., 1990). Furthermore, the usage of fuel salt also exhibits desirable properties in relation to safety (Serp, et al., 2014; Nuclear Energy Advisory Committee; Generation IV International Forum, 2002), as fuel salt usage corresponds to:

- highly negative temperature and void reaction coefficients, meaning that as temperature rises, the reaction speed slows down, making the reactor self-regulated
- low operating pressures and reduced structural stresses
- a low inventory of volatile fission products
- the possibility for fail-safe draining of the fuel salt in sub-critical tanks through the use of freeze plugs.

While MSRs are often discussed in relation to breeding with a closed thorium fuel cycle to minimize the contents of long-lasting radioactive content in waste, the fluid nature of the fuel salt together with a high neutron economy in MSRs also allow for the burning of existing transuranic actinides resulting from the uranium-plutonium cycle through the blending of actinide feeds into the fuel salt (Serp, et al., 2014). Additionally, high fuel burn-up, high flexibility in fuel choice and the possibility for breeding all promote sustainability and long-term availability of nuclear fuel. Finally, the fluid nature of the MSR allows for on-line reprocessing of fuel salt through helium bubbling and pyrochemical processes.

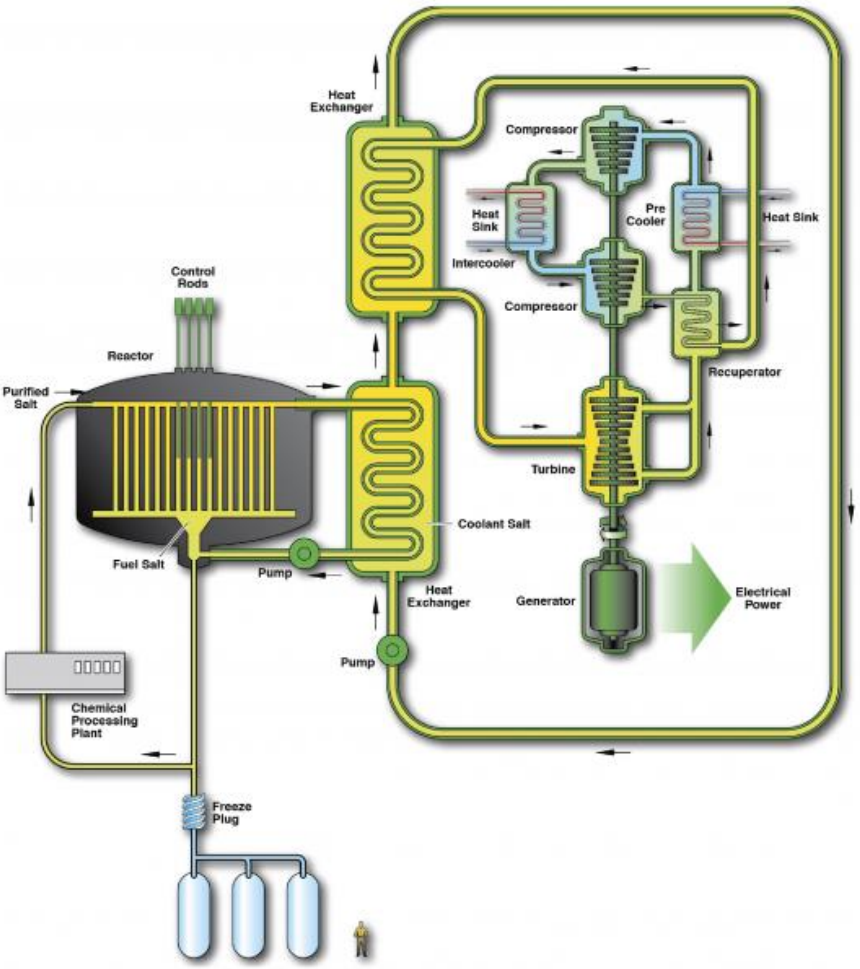

Figure 2. Illustration of a molten salt reactor concept, showing both core components and the scale of the reactor (Campbell, sd).

Research on the MSR concept can be traced back as far as in the late 1940s, when researchers at the ORNL investigated the potential use of fluid fuels in nuclear reactors. In particular, molten salts were considered due to their stability to high temperatures and radiation, as well as their heat transfer properties and the large solubility of uranium (MacPherson, 1985). However, it was not until 1954, when the first actual demonstrator of the MSR concept was realized during the military oriented Aircraft Reactor Experiment (ARE), a program dedicated to the design of nuclear-powered aircrafts. While interest in the program faded, the ARE did at the time demonstrate the chemical stability of uranium (IV)-fluoride and showed that the MSR concept was stable and self-regulating through the large thermal expansion coefficient of the fuel salt and the semi-automatic removal of gaseous fission products (Rosenthal, et al., 1969; Serp, et al., 2014). Subsequently, the promising results from the ARE led to the research and development of a number of concepts intended to be used for civil power production. The resulting program known as the Molten Salt Reactor Experiment (MSRE) operated successfully throughout the 1960s and demonstrated the viability of the MSR while also being the first reactor to use U-233 as fuel (MacPherson, 1985). Moreover, the final operating stage of the MSRE was used to conducted a series of experiments relating to various processes in the reactor, such as the stripping of xenon gas and the migration of fission products. Advancements in the reprocessing flowsheet and experience gained from both the ARE and the MSRE led to the proposal of an advanced concept, the Molten Salt Breeder Reactor. However, despite the success of the demonstrators, the MSR program was closed down in the early 1970's in favour of other concept designs (MacPherson, 1985; Serp, et al., 2014).

Currently, the Molten Salt Fast Reactor (MSFR) concept operating on a thorium cycle has been selected as the baseline concept for further research and development. While the performance of MSR has been a relatively well studied aspect, further research and development needs to be conducted on the following aspects to assess the overall viability of MSR technology (Nuclear Energy Agency; Generation IV International Forum, 2014):

- The physical-chemical behaviour of fuel salts.
- The compatibility of salt with structural materials for fuel and coolant circuits.
- The instrumentation and control of fluid salt
- On-site fuel processing

1.3 The Extraction of Fission Products from Molten Salt

One of the large advantages of the liquid nature of the fuel stems from the possibility of continuous on-line treatment and the extraction of fission products that negatively impact the performance of the reactor. The fission products generated in the fuel salt can readily be divided into three different categories according to their chemical properties within the fuel salt (Furukawa, et al., 1990):

- Rare gas elements
- Salt soluble elements (e.g. lanthanides)
- Salt insoluble elements (e.g. noble metals)

Several extraction techniques are currently being researched to separate the various classes of fission product from the fuel salt. As an example, fluorination of the molten salt may be used to extract actinides from fuel salt while electrochemical reduction and oxidation techniques may be used to extract zirconium and rare earth elements (lanthanides) (Uhlır, 2007).

An extraction technique for the removal of noble gasses, known as helium bubbling, was proposed in the early 1970s by the ORNL for use in the Molten Salt Breeder Reactor program. In this proposal, helium is injected into a bypass of the fuel salt stream through the use of Venturi type bubble generators to remove noble gasses, such as xenon and krypton, that act as neutron poisons (Gabbard, 1972). Moreover, observations made during the studying of the migration of noble metals in the MSRE program suggested that the gas-liquid interfaces inside the fuel salt stream represent stable surfaces for noble metal deposition (Kedl,

1972). It is therefore proposed is that noble metals may also be extracted through helium bubbling by a process called flotation, a process that is widely used in the mineral processing industry, the waste-water treatment industry and traditionally, the mining industry. In this way the deposition of the noble metal fission products on vital reactor circuit components would be minimized and the life-time of said components increased. However, further research needs to be done towards demonstrating the feasibility of helium bubbling for the extraction of noble metals from fuel salt and the optimization of the flotation process parameters for noble metal extraction.

2. Flotation Theory

Flotation is a separation technique used to separate materials based on their hydrophobic and hydrophilic characteristics. To this end, gas is often dispersed inside aqueous solutions to lift sufficiently hydrophobic particles through buoyancy. The technique has been widely used to separate particles of varying sizes, but is limited by its flotation extraction for fine particles, particles approximately less than 10 μm in size, and for coarse particles, particles approximately more than 100 μm in size. The low flotation extraction of these classes is often ascribed to a decrease in probability of one the fundamental sub-processes of flotation, bubble-particle collision and the chance for bubble-particle detachment not to occur respectively. The fundamental sub-processes of flotation are described in more detail in the following sections.

2.1 Elementary Processes of Fine Particle Flotation

The theory of flotation consists of a wide range of elementary processes. While physico-chemical research in flotation performed during the last few decades has resulted into a vast improvement of the theory of flotation, it was not until recently that fine particle flotation has seen a rise in interest. In particular, when fine particle flotation is considered, the flotation process can be very generally described by the following three sub-processes (Schulze, 1984):

1. The collision between bubbles and particles.
2. The attachment of particles on a bubble and the formation of a thin film between the two.
3. Thinning and rupturing of the film and the formation of stable bubble-particle aggregates.

The bubble-particle collision process is characterized by the number of particles in the bubble trajectory that collide with the bubble. As such, this process is largely dependent on the collision cross-section of the bubble and the trajectories of the individual particles. Fortunately, it can be shown that for sufficiently small particles, particles approximately smaller than 50 μm in size, inertial forces can be neglected, meaning that the particle trajectories are completely dependent on the viscous forces resulting from the flow regime around the bubble (Yoon & Luttrell, 1989).

After a particle collides with a bubble, a thin film is formed between the two (Yoon & Luttrell, 1989). The particle then slides alongside the boundary of the bubble for a certain amount of time t_s, the sliding time, depending on the angle at which a particle hits the bubble (Yoon & Luttrell, 1989). While sliding, the film is gradually thinned and drained until the film reaches a critical thickness and ruptures (Yoon & Luttrell, 1989). The minimum time required to thin and rupture the film is known as the induction time t_i. If the sliding time is longer than the induction time, a primary hole is formed which allows for the formation of a three-phase contact (Schulze, 1984).

2.2 The Chemical Kinetic and Probabilistic Mixed Model

As mentioned by Schulze, modelling of the flotation process has been approached from various angles, including: chemical kinetic, probabilistic and mixed models (Schulze, 1984). Underlying some mixed kinetic models, models in which the processes in a flotation machine are described by combining concepts used in chemical kinetics and the probabilities of the underlying elementary processes in flotation, is the assumption that the rate of bubble-particle aggregate formation and disintegration can be expressed as a kinetic equation in the form (Schulze, 1984; Prakash, et al., 2018):

$$\frac{dc_p}{dt} = Kc_p^j c_b^k \quad (1)$$

where c_p is the particle concentration, c_b is the bubble concentration, K the flotation rate constant and j, k are the orders of the concertation terms. According to Yoon and Mao (Yoon & Mao, 1997), previous research performed by Sutherland, Tomlison and Fleming has shown that mineral flotation can be described as a first-order process. This finding combined with a constant gas flow rate, meaning that the change in bubble concentration is neglectable, allows for the above kinetic equation to be reduced to (Prakash, et al., 2018):

$$\frac{dc_p}{dt} = Kc_p \quad (2)$$

The probability of a particle being successfully floated is often expressed as the product of the probabilities of the elementary sub-processes. Specifically, this probability is given by (Schulze, 1984; Yoon & Luttrell, 1989):

$$P_f = P_c P_a (1 - P_d) \quad (3)$$

where P_c is the probability of bubble-particle collision, P_a is the probability of bubble-particle adhesion and P_d is the probability of bubble-particle detachment. Furthermore, non-correlation between these probabilities is assumed. In case fine particle flotation is considered, the probability of detachment can be omitted, as the inertial forces that play a large role in the detachment probability become sufficiently small to the point where the probability of detachment is zero by approximation (Yoon & Luttrell, 1989).

A number of models have been derived by various researchers for the bubble-particle collision probability (Prakash, et al., 2018). Generally, the relation between the bubble-particle collision probability and the ratio between the particle diameter and the bubble diameter can be expressed in the form (Yoon & Luttrell, 1989; Prakash, et al., 2018):

$$P_c = A\left(\frac{d_p}{d_b}\right)^n \quad (4)$$

where d_p is the particle diameter and d_b the bubble diameter. In particular, Yoon and Lutrell have developed fine particle flotation models for both the bubble-particle collision probability and the bubble-particle adhesion probability for different flow conditions by deriving the particle trajectories using the Stokes- and potential stream functions (Yoon & Luttrell, 1989). Furthermore, an intermediate flow condition model was derived from an empirical stream function. The intermediate model has been shown the hold up well for Reynold number smaller than 100. However, whether the intermediate model holds for larger Reynold numbers is uncertain (Yoon & Luttrell, 1989).

Table 2. Bubble-particle collision probability model derived by Yoon and Lutrell (Yoon & Luttrell, 1989).

Flow Conditions	$\boldsymbol{A}$	$\boldsymbol{n}$
Stokes ($\boldsymbol{Re \ll 1}$)	$\frac{3}{2}$	*2*
Intermediate	$\frac{3}{2} + \frac{4Re_b^{0.72}}{15}$	*2*
Potential ($\boldsymbol{Re \gg 100}$)	*3*	*1*

The aforementioned bubble-particle adhesion probability model is given by (Yoon & Luttrell, 1989):

$$P_a = \sin^2\left[2 \arctan \exp\left\{\frac{-3u_b t_i}{2r_b\left(r_b/r_p+1\right)}\right\}\right] \quad (5)$$

for the Stokes flow conditions,

$$P_a = \sin^2\left[2 \arctan \exp\left\{\frac{-(45+8Re^{0.72})u_b t_i}{30r_b\left(r_b/r_p+1\right)}\right\}\right] \quad (6)$$

for the intermediate flow conditions, and

$$P_a = \sin^2\left[2 \arctan \exp\left\{\frac{-3u_b t_i}{2\left(r_b+r_p\right)}\right\}\right] \quad (7)$$

for the potential flow conditions. In these equations, u_b is the bubble rise velocity, r_b the bubble radius and r_p the particle radius. The stationary bubble rise velocity is expressed by Schulze as (Schulze, 1984):

$$|u_b| = \sqrt{\frac{4g d_b}{3c_d}} \quad (8)$$

where g is the gravitational acceleration and c_d the drag coefficient of the bubble. Alternatively, if the Reynold number of the bubble is less than 0.5, the drag coefficient may be approximated by:

$$c_d = \frac{24}{Re} \quad (9)$$

Finally, the relation between the first-order flotation rate constant and the probability of successful flotation is expressed by Yoon as a function of the superficial gas u_{sg}, the probability of a particle being successfully floated and the bubble diameter (Yoon, 1993).

$$K = \left(\frac{3P_f}{d_b}\right)u_{sg} \quad (10)$$

2.3 Design Parameters for Flotation Processes

Since intermediate flow condition are most applicable to column flotation (Yoon, 1993), equations (4) and (6) are mostly considered for the optimization of the flotation rate constant as expressed in equation (10). Concluding from these equations, the following parameters can be influenced to alter the flotation rate:

1. the bubble diameter d_b,
2. and the superficial gas velocity u_{sg}.

2.3.1 Bubble Size

When considering the relation between the bubble diameter and the flotation rate for intermediate flow conditions, the collision probability is seen to be roughly inversely proportional to the bubble diameter for large Reynold numbers and inversely proportional to the squared bubble diameter for small Reynold numbers. However, a decrease in bubble size generally also increases the probability of adhesion due to an increase in the sliding time t_s, by lowering the bubble rise velocity u_b (Yoon & Luttrell, 1989). A further decrease in bubble size results in a decrease in the sliding time t_s by lowering the sliding distance (Yoon & Luttrell, 1989). Furthermore, there is an additional inversely proportional diameter term in equation (10). Thus, combining the two models, the bubble size appears to be of great importance for the flotation rate and while overall, the flotation rate increases with decreasing bubble size, there appears to be an optimal bubble size after which a further decrease in bubble size decreases the flotation rate due to a decrease in adhesion probability.

2.3.2 Gas Holdup

The gas holdup of a multi-phase system can be described as the volumetric gas content of a system. According to Prakash et al. (Prakash, et al., 2018), the gas holdup is dependent on the bubble characteristic, the flow characteristic and the bubble rise velocity. Furthermore, the gas holdup is reportedly an important parameter for the extraction of particles in a column flotation system when combined with flow regime data (Prakash, et al., 2018). Recently, studies on column flotation by Massinaei et al. (Massinaei, et al., 2009), have shown a linear relation between the gas holdup and the bubble surface area flux S_b, which is related to the bubble size and the superficial gas velocity by:

$$S_b = \frac{6u_{sg}}{d_b} \qquad (11)$$

Thus, for a constant bubble size the gas holdup is also expected to show a linear correlation with the superficial gas velocity. Similar to the flotation rate equation derived by Yoon (10), a linear relation between the collection zone rate constant and the gas holdup has been observed (Massinaei, et al., 2009), which means that for a constant bubble size, there is a linear relation between the collection zone rate constant and the superficial gas velocity.

The superficial gas velocity is linearly correlated to the flotation rate according to equation (10). However, the impact of the superficial gas velocity on the flow regime should also be considered. For low superficial gas velocities, the flow regime is characterized by a homogeneous bubbly flow in which formed bubbles do not coalesce or breakup. In contrast, at high superficial gas velocities, the flow regime becomes heterogeneous and, depending on the flotation column diameter, is either characterized by the slug flow regime or the Churn-turbulent flow regime (Prakash, et al., 2018). It can be readily conceived that the heterogeneous nature of these high superficial gas velocity regimes alongside the wide variance in bubble size are undesirable for column flotation.

3. Methodology

Investigation of the relevant flotation parameters is performed in this study through the use of an experimental fluid loop. In this loop, simulants are used to replicate the MSR conditions during reactor operation. The following section contains a detailed description of the experimental setup and the measurement procedures used for the evaluation of the correlation between: the flotation parameters, the mean bubble size, the average gas holdup and the fine particle extraction in a flotation column.

3.1 Experimental Setup

The experimental setup used for the study mostly consists of polyvinyl chloride tubing and includes some transparent Plexiglass elements. The transparent components correspond to the two main components in this setup, namely the bubble generator and the flotation column, which are described in detail in the following section. The pumping action is provided for by a MIDA Nastec pump and the fluid flow rate is adjusted directly through the pump and through the manual valve mounted above the pump. Monitoring of the fluid flow is performed through an Endress+Hauser Promag 10 flow meter that is linked to a desktop computer running LabVIEW software. Additionally, to limit the effect of temperature changes on the flow characteristics of the setup, a SWEP 312LX20/1P-SC-S heat exchanger is used to divert excess heat that is generated by the pump. Images of the complete setup can be seen in Figures 3 and 4.

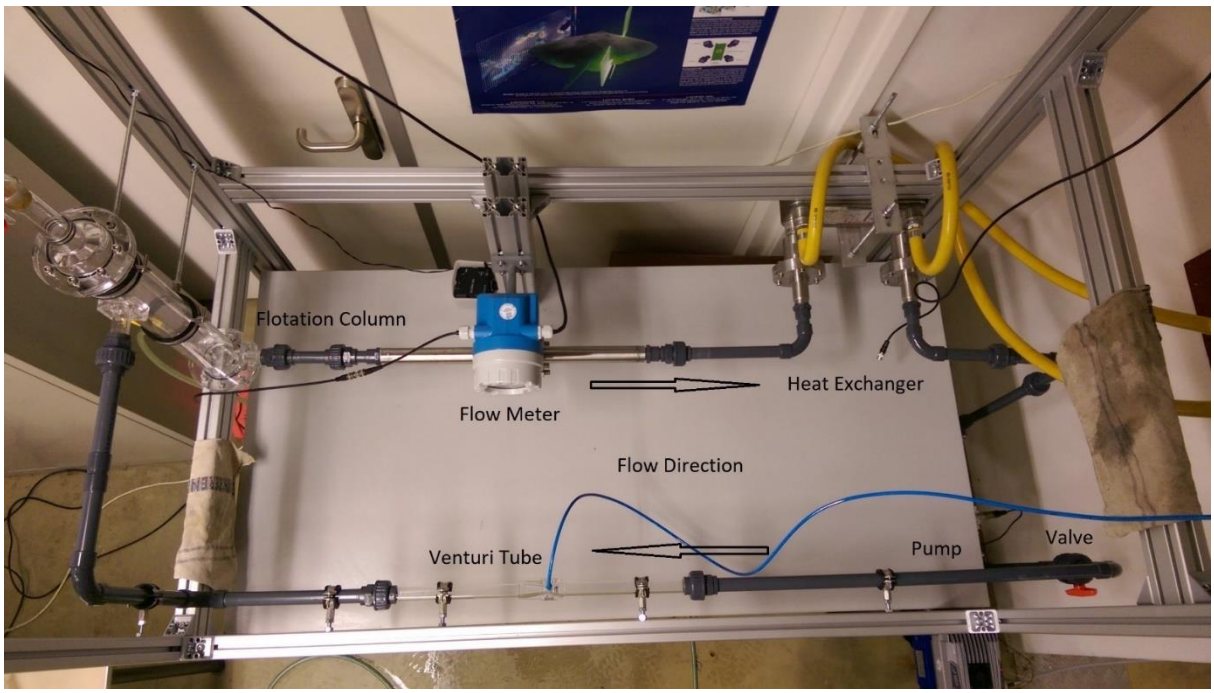

Figure 3. Top view of the experimental setup.

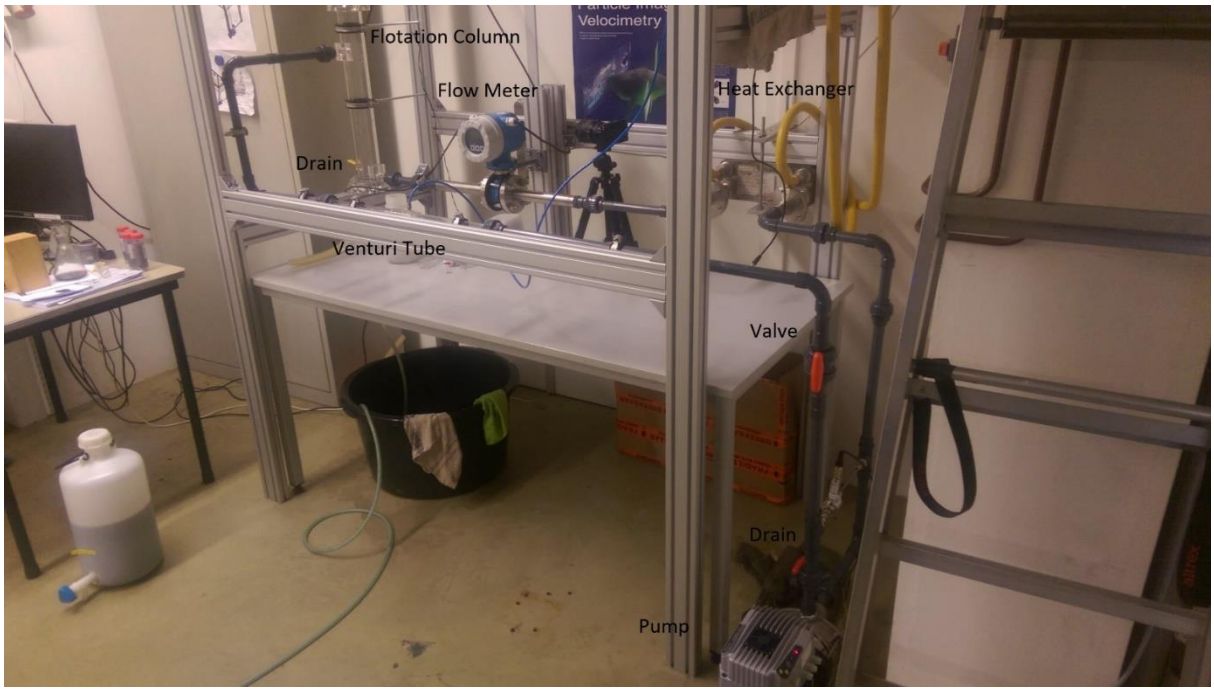

Figure 4. Side view of the experimental setup.

3.1.1 Bubble Generator

A Venturi type bubble generator (Figure 5) is used to inject compressed air into the fluid stream that leads to the flotation column inlet. The main advantage of using a Venturi tube over other methods is its simplistic nature compared to other conventional bubble generator design, as its design does not feature any intricate parts nor does it require an external power supply to operate. The actual design is similar to one of the concepts produced by C. H Gabbard for use in a molten salt breeder reactor concept (Gabbard, 1972). It features a 7.5 degrees smooth bore diffuser cone, where gas is radially injected into the low-pressure throat of the Venturi tube. In the Venturi tube, the formation of fine bubbles occurs due to the fluid turbulence that is present in the diffuser cone, and is thus dependent on the local pressure differences or alternatively, the fluid flow, as described by the Venturi effect.

The supply of compressed air is handled through a Bronkhorst EL-FLOW Select mass flow controller. FlowDDE software is used to facilitate the connection between FlowView, a Windows application used to measure and set the gas throughput of the controller, and the controller itself.

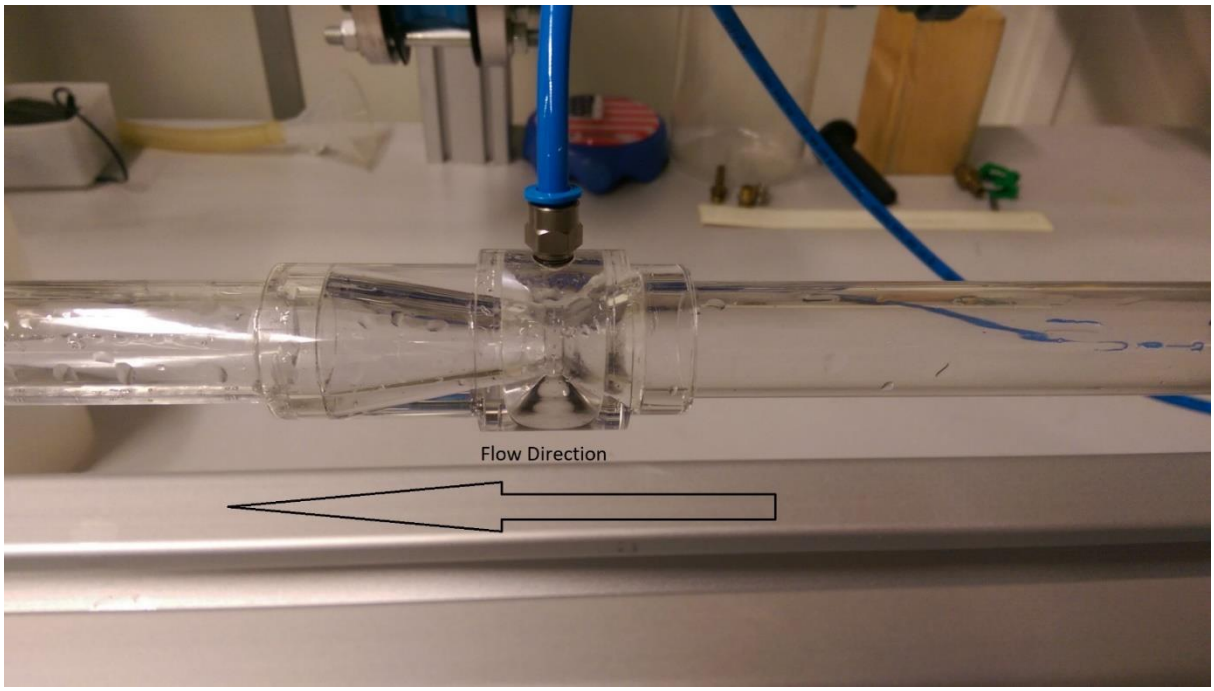

Figure 5. The Venturi style bubble generator.

3.1.2 Flotation Column

The main setup component is the Plexiglass flotation column (Figure 6). The fluid flow inlet is situated on the upper portion of the Plexiglass flotation column, while the outlet is at the bottom. A modified glass Hallimond tube is mounted on the top side of the flotation column to collect the molybdenum particles that have floated to the gas-fluid interface. In order to facilitate the collection of the aforementioned particles, there is an additional reservoir attached to the underside of the Hallimond tube slope. This reservoir can be completely drained by turning the valve at its bottom. Following previously performed experimental research with fine particle flotation, the Hallimond tube curve has been determined to perform optimally for a 115 degrees curve, as such, a 115 degrees curve is featured in this design. At this angle, bubble-particle detachment due to wall collisions is reported to be minimal.

Figure 6. The flotation column and the top mounted Hallimond tube.

3.1.3 Simulants

Simulants are used to resemble the flow characteristics of molten salts as closely as possible. To this end, a water-glycerol mixture is used having a similar kinematic viscosity to the LiF-BeF_2-ThF_4 (71.7-16-12.3 mol%) mixture. The volume ratio of glycerol to water that is required to achieve this is calculated through a web-based tool based on the parameterisation in Cheng (Cheng, 2008). Table 3 displays some of the properties of the molten salt mixture and the simulant fluids.

Table 3. Physico-chemical properties of the simulant fluids and the targeted molten salt composition (Cheng, 2008; Capelli, et al., sd).

Composition	*Density* $[g/cm^3]$	*Dynamic viscosity* $[mPa \cdot s]$	*Kinematic viscosity* $[mm^2/s]$	*Temperature* $[K]$
LiF-BeF_2-ThF_4 (71.7-16-12.3)	*3.342*	*10.703*	*3.202*	*900*
Water	*0.99805*	*1.0049*	*1.0068*	*293*
Glycerol	*1.2608*	*1413.8*	*1121.4*	*293*
Water-glycerol (66.6-33.3 vol%)	*1.0956*	*3.4825*	*3.1786*	*293*

To simulate the occurrence of noble metals in molten salt reactors, molybdenum particles of different sizes are added to the water-glycerol mixture before each experiment. In particular, a similar molybdenum concentration is used to the equilibrium concentration of molybdenum in a single-region MSR that was calculated in an ORNL publication by W.L. Carter (Carter, 1968). The aforementioned equilibrium concentration was calculated to be 6.006 g/ft^3, or roughly 0.2121 g/l. The total volume of the experimental setup is estimated to be 5 l, as such around 1.061 grams of molybdenum is weighed on a semi-micro balance for each experiment.

3.2 Bubble Size Measurement Procedure

The mean bubble size produced in the Venturi tube as a function of the different flow parameters, was determined by a photographic technique. The pictures are taken at the Venturi tube outlet, right after the bubble formation, using a NIKON J5 camera with a NIKON AF-S DX Micro Nikkor 40mm f/2.8G lens. As the nature of high-speed photography leads to the production of fairly dim pictures, a Godox LED64 Video Light is used as additional backlighting. Images were taken for a range of different gas flows and fluid flows to determine the correlation between these flotation parameters and the average bubble size formed. For each parameter combination, the setup was given around half an hour to reach equilibrium conditions and a total of ten pictures were taken per combination. Figure 7 shows the measurement setup and the location at which the images were taken.

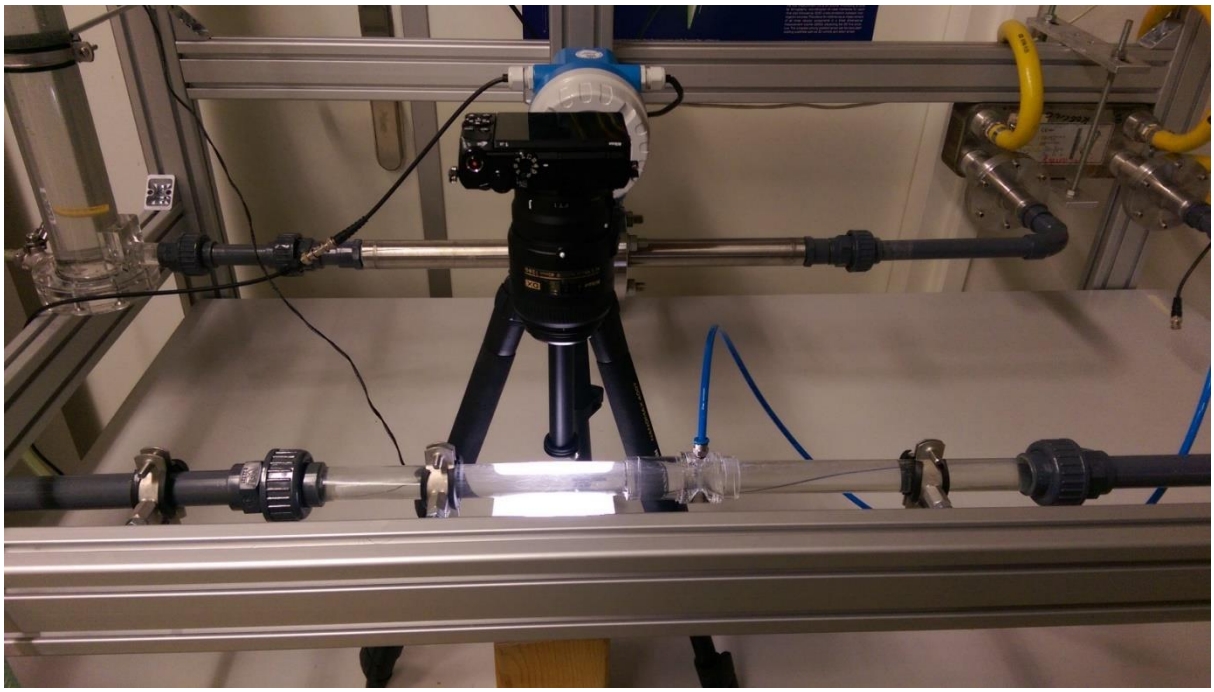

Figure 7. Setup for the bubble size measurements.

3.2.1 Image Processing

Bubble images are analysed with ImageJ software, an open source image processing program. Firstly, each image is correctly scaled against the tube width seen in the images and the sides of the images are cropped. After scaling the images, bubble contours are enhanced and the images are converted to binary masks through thresholding. These masks are evaluated with an extension called ellipse split. Subsequent, data resulting from this process is then compiled and stored in Excel. While different images require slightly altered

scripts, a general script can be found in Appendix A. Following from the data generation, the equivalent spherical diameter is calculated for each bubble from the surface area A of each bubble:

$$d_{eq} = \sqrt{\frac{4A}{\pi}} \tag{12}$$

The final distribution in bubble size is expressed as the Sauter mean diameter, the volume/surface mean or the equivalent diameter for which a mono-dispersed collection of particles with diameter d_{32} has an identical total surface area and total volume to the original particle collection (Kowalczuk & Drzymala, 2016):

$$d_{32} = \frac{\sum n_i d_{eq,i}^3}{\sum n_i d_{eq,i}^2} \tag{13}$$

3.3 Average Gas Holdup Measurement Procedure

The average gas holdup is measured by observing the relevant height differentials in the smaller upper section of the flotation column while increasing the gas flow from 0 to 50 cm^3/min in steps of 10 cm^3/min, as indicated in Figure 8. During each incremental change, the setup was given half an hour to reach equilibrium conditions. For each change in gas flow, a before and after image was taken with the same setup as described in the bubble size measurement procedure section and both images were layered on top of each other using Image editing software. The resulting images were imported into ImageJ to scale the images and to measure the relative change in gas-fluid interface height. Resulting data is expressed as the relative change in fluid volume compared to the ungassed experiment. Consequently, the average gas holdup is expressed as:

$$\varepsilon_g = \frac{1}{4}\pi d_c^2 \Delta h \tag{14}$$

where d_c is the diameter of the relevant column section and Δh is the relative change in height compared to the ungassed measurement height.

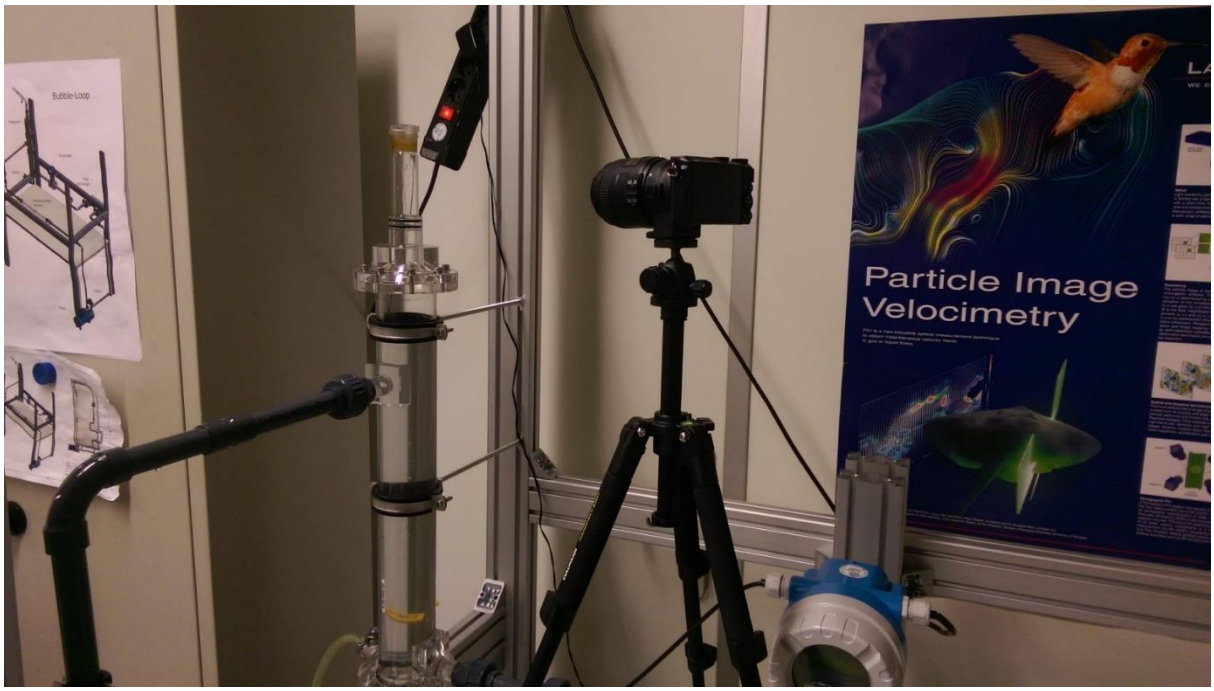

Figure 8. Setup for the gas holdup measurements.

3.4 Fine Particle Extraction Measurement Procedure

Before the particle extraction measurements are performed, the water-glycerol mixture is poured into the setup from the top side of the flotation column. Thereafter, the setup is degassed by letting the setup run at roughly 0.5 l/s for at least an hour. Subsequently, the pump, the valve and the gas controller are adjusted to set the desired parameters and the setup is left to run for an additional half an hour to reach equilibrium conditions. After the desired conditions have been met, molybdenum particles, that are stored in a glass Erlenmeyer flask are brought into suspension and emptied in the upper section of the flotation column. The Erlenmeyer flask is rinsed and emptied several times with water-glycerol until the majority of the particles are visibly removed from the container. Subsequently, the Hallimond tube is mounted and the water-glycerol content is increased until the gas-fluid interface completely covers the highest point of the reservoir (as depicted in Figure 9).

Figure 9. Particle extraction experiment right after adding the particles and mounting the Hallimond tube.

The sampling is performed by draining the reservoir completely until it is emptied into a 50 ml sample tube, the Hallimond tube is then rinsed to liberate some of the particles that have settled on the glass surfaces and is then emptied once again. Samples are taken each half an hour for two hours in total, resulting in four samples per experiment run. After all samples have been collected, the Hallimond tube is rinsed four more times and emptied into a Erlenmeyer flask. This final sample is referred to as the Hallimond tube residue. Finally, the remaining water-glycerol is drained and emptied into a plastic container through the use of both drains and the setup is filled and ran with demineralized water to remove most of the residual particles that have been deposited inside the setup.

All five sample tubes are emptied in smaller 14 ml tubes and thoroughly rinsed with ethanol the remove all the particles. Particles are then separated from the water-glycerol by putting the sample tubes inside a Jouan B3.11 Centrifuge at 3000 rpm for five minutes. Repeating this procedure allows for reducing the number of small sample tubes to only five tubes. After which, the samples are emptied in crucibles and heated on a VMS-A magnetic hotplate stirrer. When the ethanol is completely evaporated, the crucibles are weighed and the resulting weight data are stored and compiled in Excel. The entire process is repeated for several different flotation parameter combinations with regards to particle size, fluid flow and gas flow. The used water-glycerol mixture is purified between each run through vacuum filtration of the mixture, using a Schleicher & Schuell grade 595 filter.

4. Results

The results from the experiments described in the methodology section are laid out in this section. Firstly, the correlation between the Sauter mean diameter of the bubble size distribution and both the gas- and fluid flow rate is reported. Secondly, results from the mean gas holdup measurements are displayed in graph form. Finally, the influences of the gas flow rate, fluid flow rate and particle size on the molybdenum particle extraction efficiency are explored.

4.1 Flotation Parameter Dependency of the Mean Bubble Size and the Gas Holdup

The results from the image analysis, described in section 3.2, are reported in Figure 10 and 11. Figure 10 shows the Sauter mean diameter as function of the fluid flow rate at a fixed gas flow rate while Figure 11 shows the Sauter mean diameter as function of the gas flow rate at a fixed fluid flow rate.

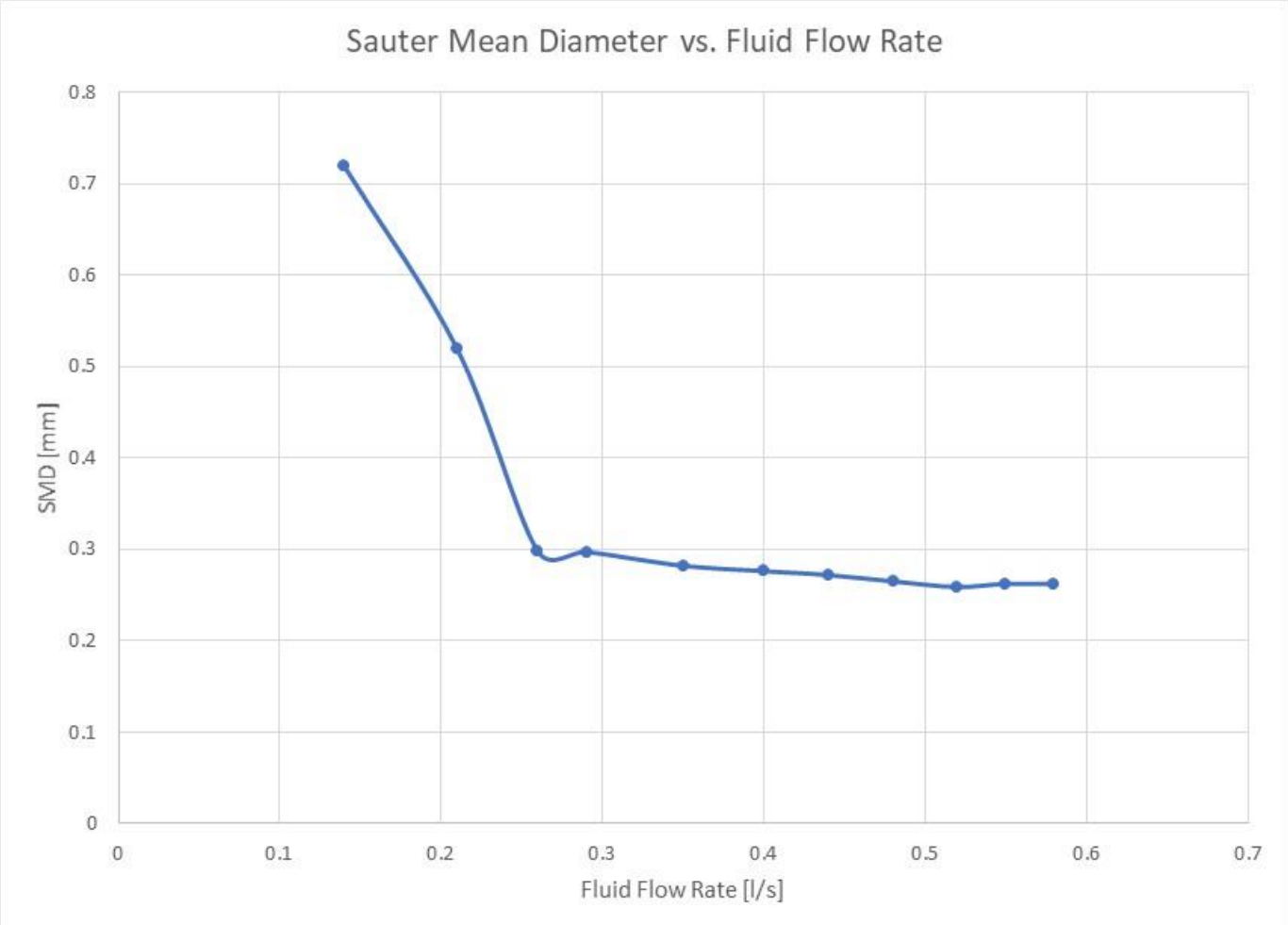

Figure 10. The Sauter mean diameter plotted against the fluid flow rate for a constant gas flow rate of 10 cm^3/min.

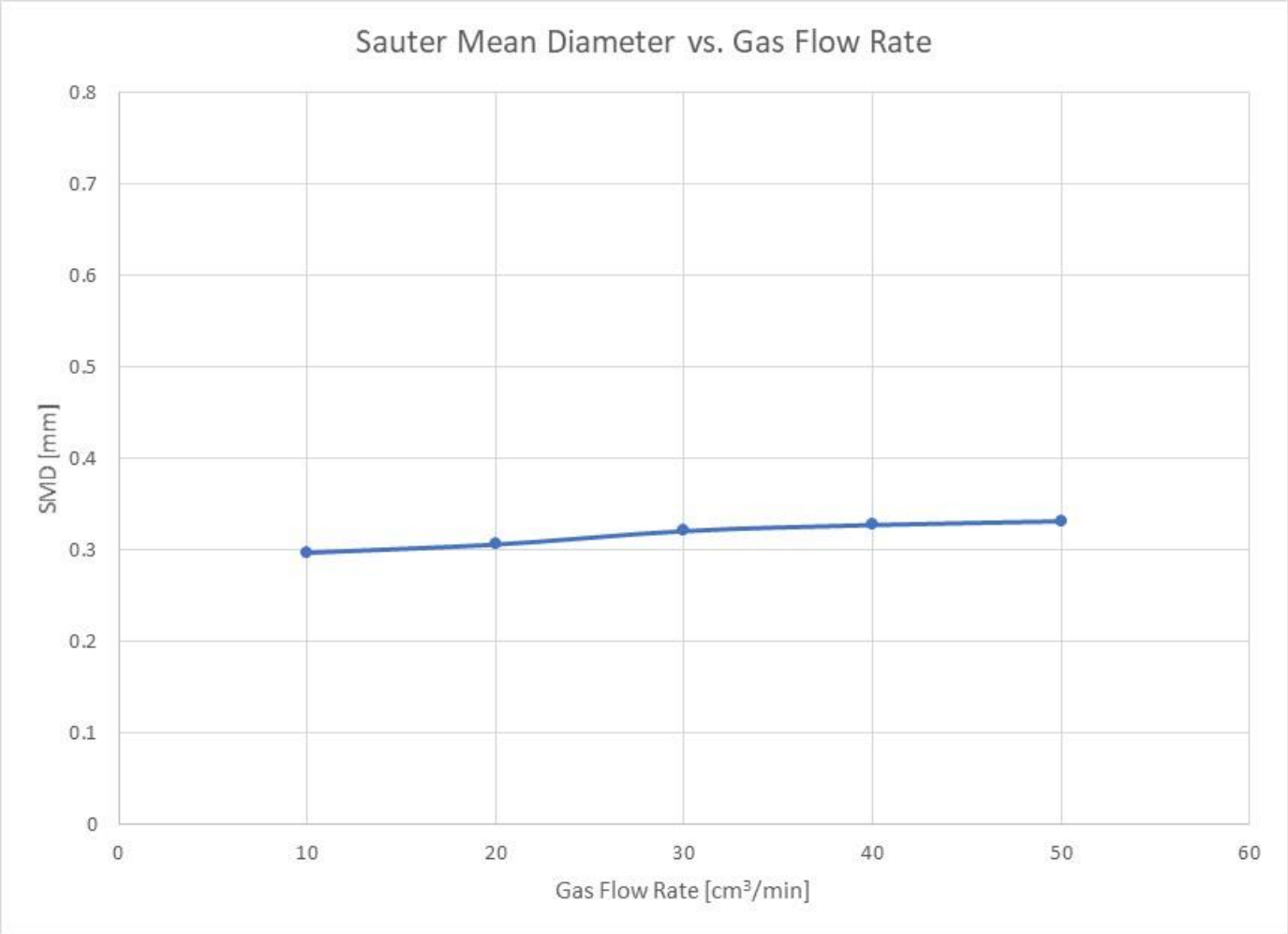

Figure 11. The Sauter mean diameter plotted against the gas flow rate for a constant fluid flow rate of 0.29 l/s.

The second important design parameter in a flotation setup is the gas holdup. This was determined experimentally for the loop used in this project and the results are shown in Figure 12 as a function of the gas flow rate. Results from the mean gas holdup measurements are expressed as the cumulative volume increase compared to the ungassed measurement.

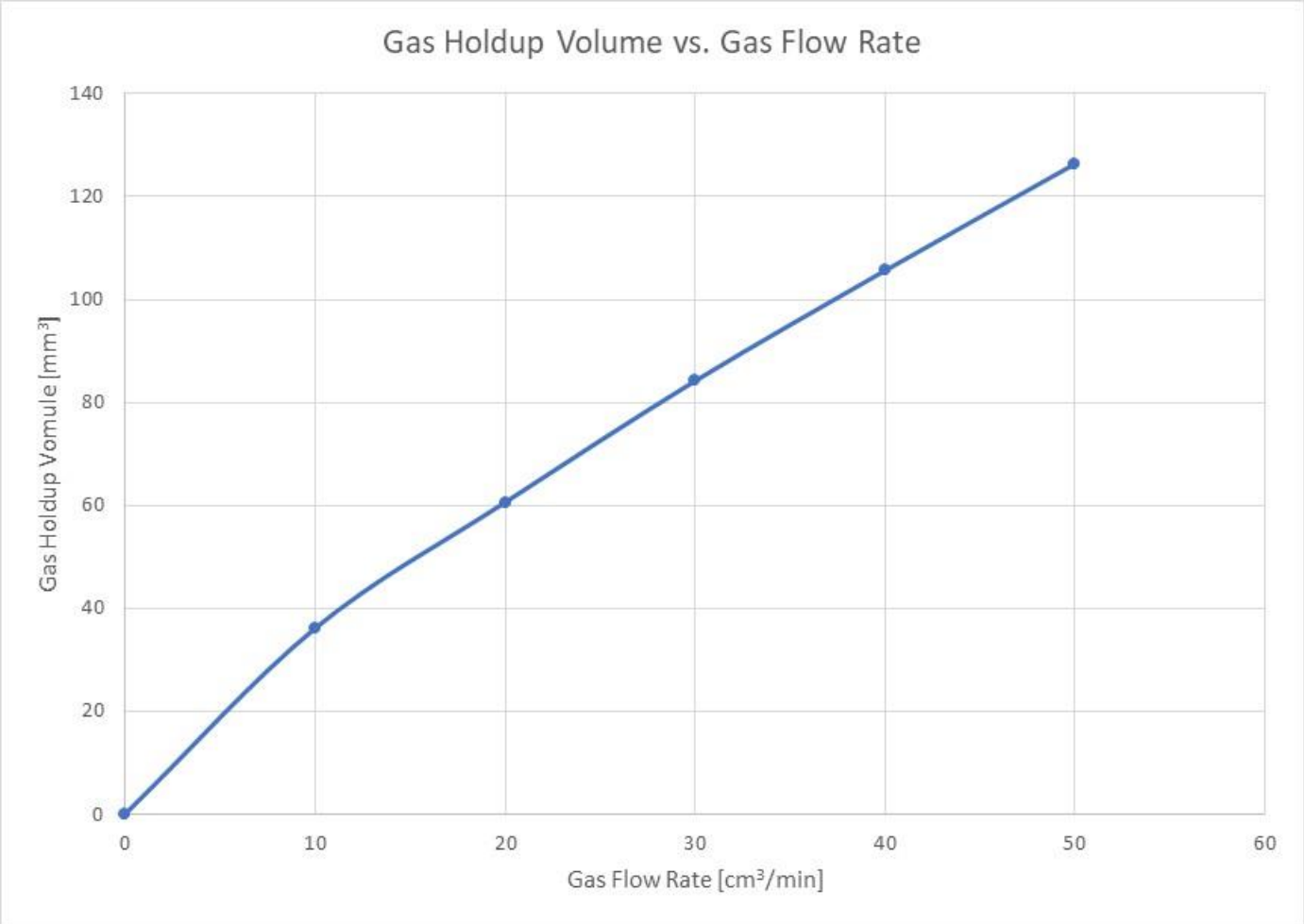

Figure 12. The mean gas holdup vs the gas flow rate for a constant fluid flow rate of 0.40 l/s.

4.2 Fine Particle Extraction

A set of experiments were performed to evaluate the fine particle extraction efficiency of two molybdenum particle sizes, 3-7 micron and 1-2 micron respectively, for various fluid flow rates and fixed gas flow rates of 10 cm^3/min and 50 cm^3/min. Finally, another experiment was performed to evaluate the fine particle extraction efficiency of nanoparticles, particles of similar size to the ones found in fuel, for flotation parameters that have been determined to be optimal for the other experiments. Consequently, based on the results laid out in this section, the nanoparticle experiment was performed for a gas flow rate of 50 cm^3/min and a fluid flow rate of 0.50 l/s.

4.2.1 Time Dependency of Fine Particle Extraction

Figures 13-15 show the time dependence of the molybdenum fine particle cumulative extraction for various gas flow rates, fluid flow rates and particle sizes. Results have been grouped by particle size as to allow for a direct comparison between the flotation parameters for different particle sizes. Additionally, the data is also displayed in Table 4. It is important to note, that the residue samples were excluded for the time dependent graphs.

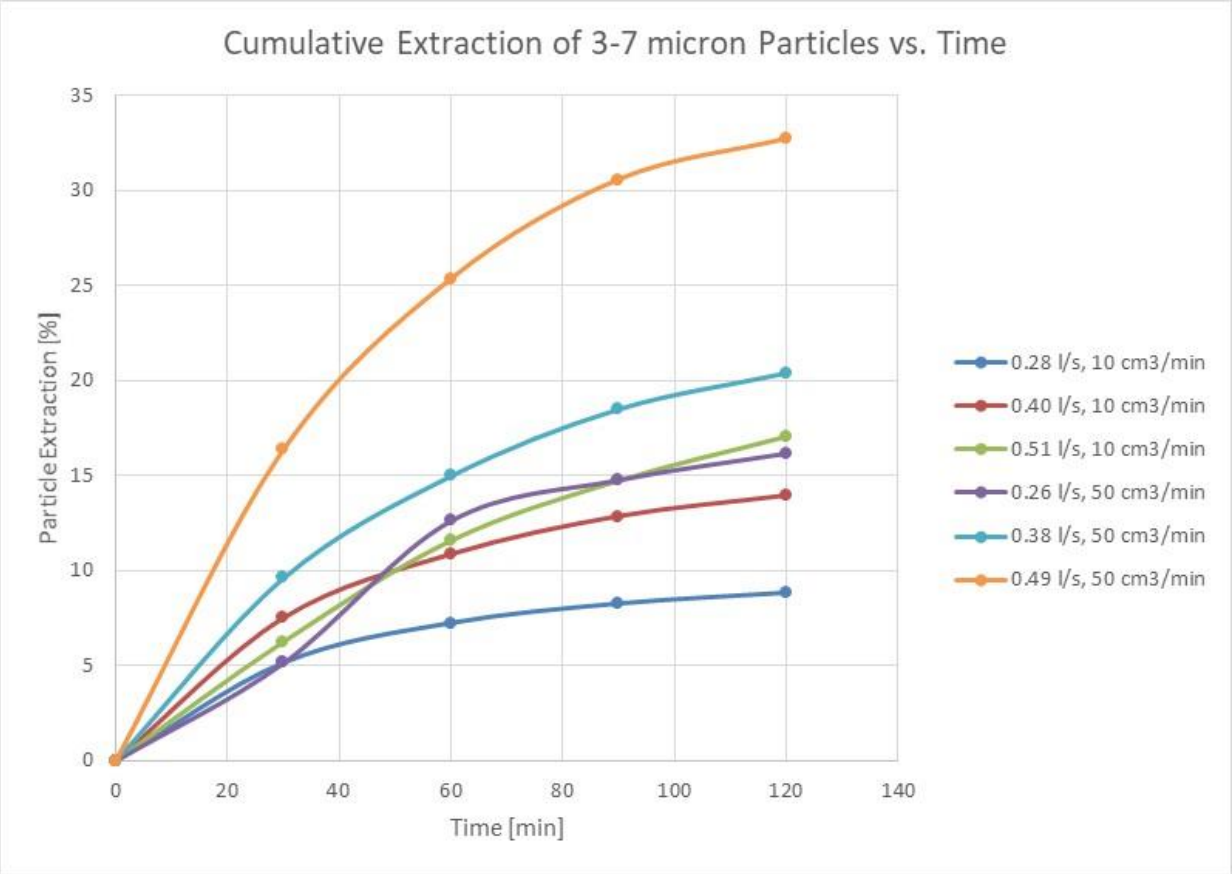

Figure 13. Cumulative extraction of 3-7 micron particles plotted against time for various gas- and fluid flow rates.

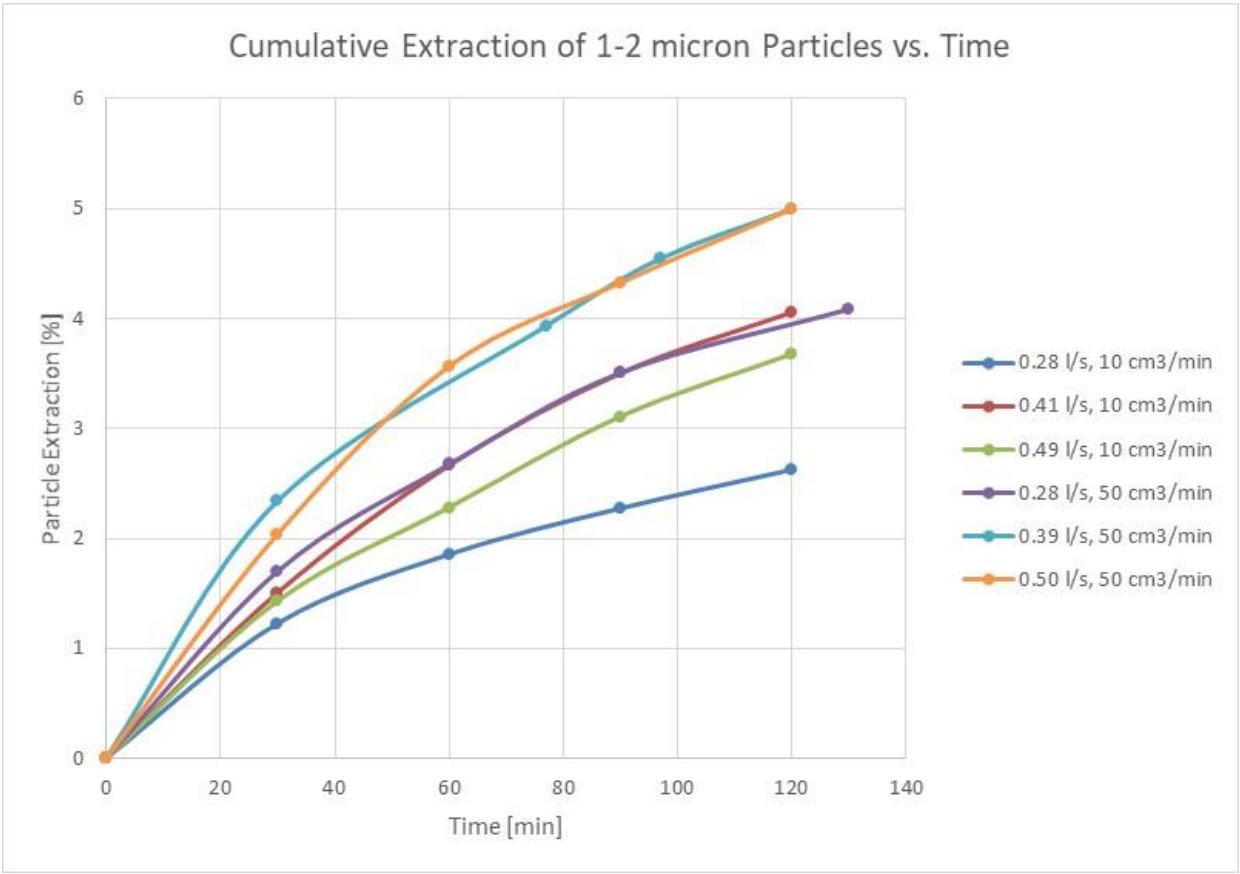

Figure 14. Cumulative extraction of 1-2 micron particles plotted against time for various gas- and fluid flow rates.

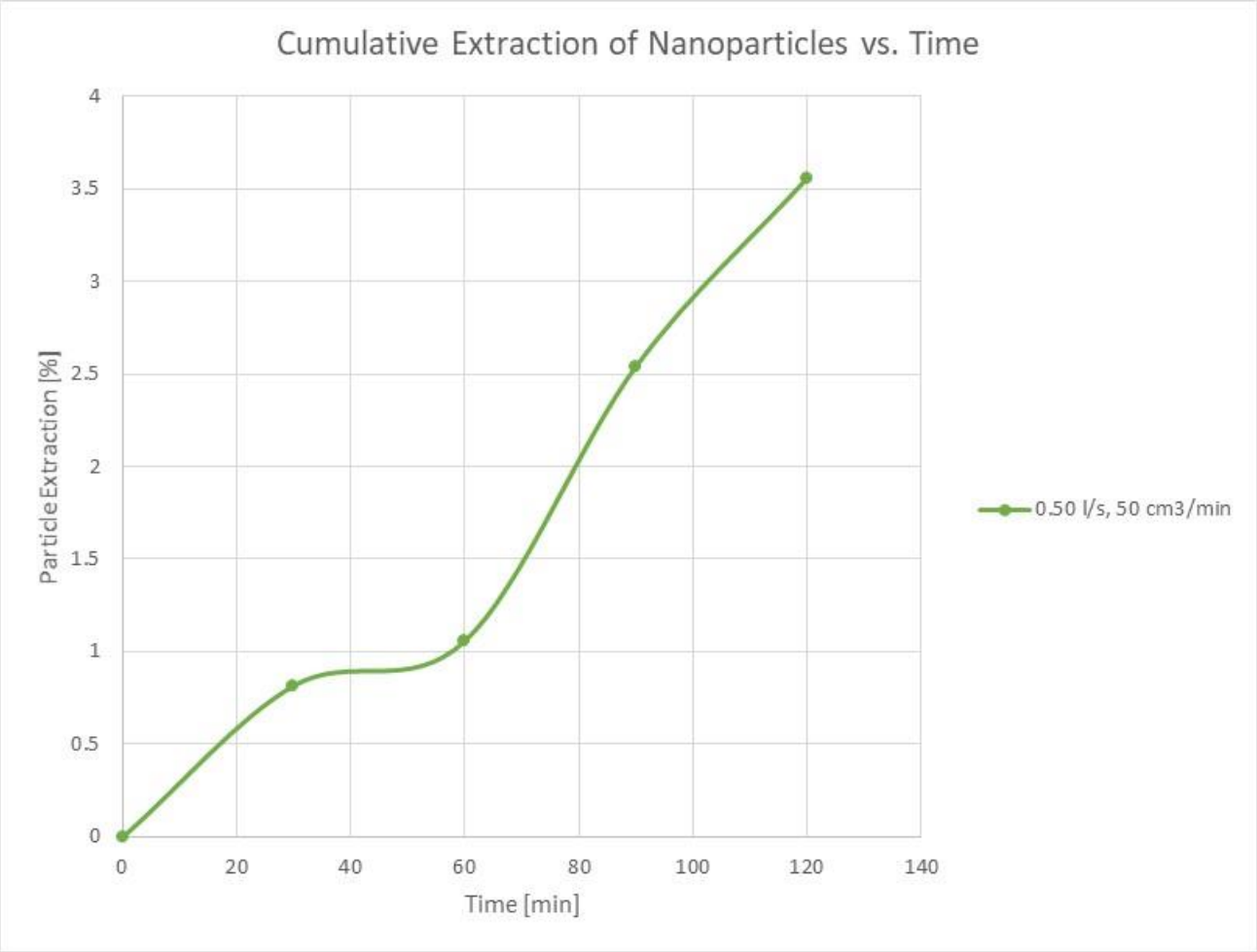

Figure 15. Cumulative extraction of nanoparticles plotted against time for a fluid flow rate of 0.50 l/s and a gas flow rate of 50 cm^3/min.

Table 4. Relative particle extraction per experiment.

Experiment	Sample 1 [%]	Sample 2 [%]	Sample 3 [%]	Sample 4 [%]	Residue [%]	Total ex. Residue [%]	Total inc. Residue [%]
3-7 micron,10 cm^3/min , 0.28 l/s	5.15	2.09	1.02	0.56	0.53	8.81	9.35
3-7 micron, 10 cm^3/min, 0.40 l/s	7.51	3.35	1.99	1.09	0.80	13.93	14.74
3-7 micron, 10 cm^3/min, 0.51 l/s	6.28	5.33	3.16	2.32	2.17	17.08	19.26
3-7 micron, 50 cm^3/min, 0.26 l/s	8.23	4.41	2.16	1.40	2.12	16.20	18.32
3-7 micron, 50 cm^3/min, 0.38 l/s	9.62	5.39	3.52	1.90	1.121	20.42	21.55
3-7 micron, 50 cm^3/min, 0.49 l/s	16.34	8.99	5.22	2.15	1.70	32.74	34.44
1-2 micron, 10 cm^3/min, 0.28 l/s	1.23	0.63	0.42	0.35	0.77	2.63	3.40
1-2 micron, 10 cm^3/min, 0.41 l/s	1.51	1.16	0.84	0.55	0.58	4.06	4.63
1-2 micron, 10 cm^3/min, 0.49 l/s	1.43	0.85	0.83	0.57	0.71	3.67	4.38
1-2 micron, 50 cm^3/min, 0.28 l/s	1.70	0.97	0.83	0.58	1.38	4.09	5.47
1-2 micron, 50 cm^3/min, 0.39 l/s	2.34	1.59	0.61	0.45	0.68	4.97	5.68
1-2 micron, 50 cm^3/min, 0.50 l/s	2.03	1.52	0.76	0.67	1.87	4.99	6.86
nanoparticles, 50 cm^3/min, 0.50 l/s	0.82	0.24	1.48	1.01	2.07	3.55	5.63

During the experiments, a significant amount of frothing was observed for the first sample of the “3-7 micron, 0.51 L/s, 10 cm^3/min” experiment and for all the “1-2 micron 0.49 l/s, 10 cm^3/min” experiment samples. When excess frothing occurs, particles suspended in the froth layer rise and deposit in the Hallimond tube extension, attaching to the glass walls as they dry up. These particles are considered lost, as rinsing the glass surface with ethanol proved to be ineffective for detaching these particles. Furthermore, the amount of froth during the latter instance was significant enough to completely fill the and escape the Hallimond tube extension. An effort was made to capture most of the escaped froth in the residue sample, however, a relevant portion of the escaped froth was still lost. Finally, a number of particles were still observed to be in the molybdenum flask during the nanoparticle experiment.

4.2.2 *Fluid Flow Rate Dependency of Fine Particle Extraction*

The fluid flow rate dependency on molybdenum particle extraction is displayed in Figures 16 and 17. While the number of data points is limited, conclusions can still be drawn with regards to the efficiency of fine particle extraction in relation to the fluid flow rate, the gas flow rate and the particle size.

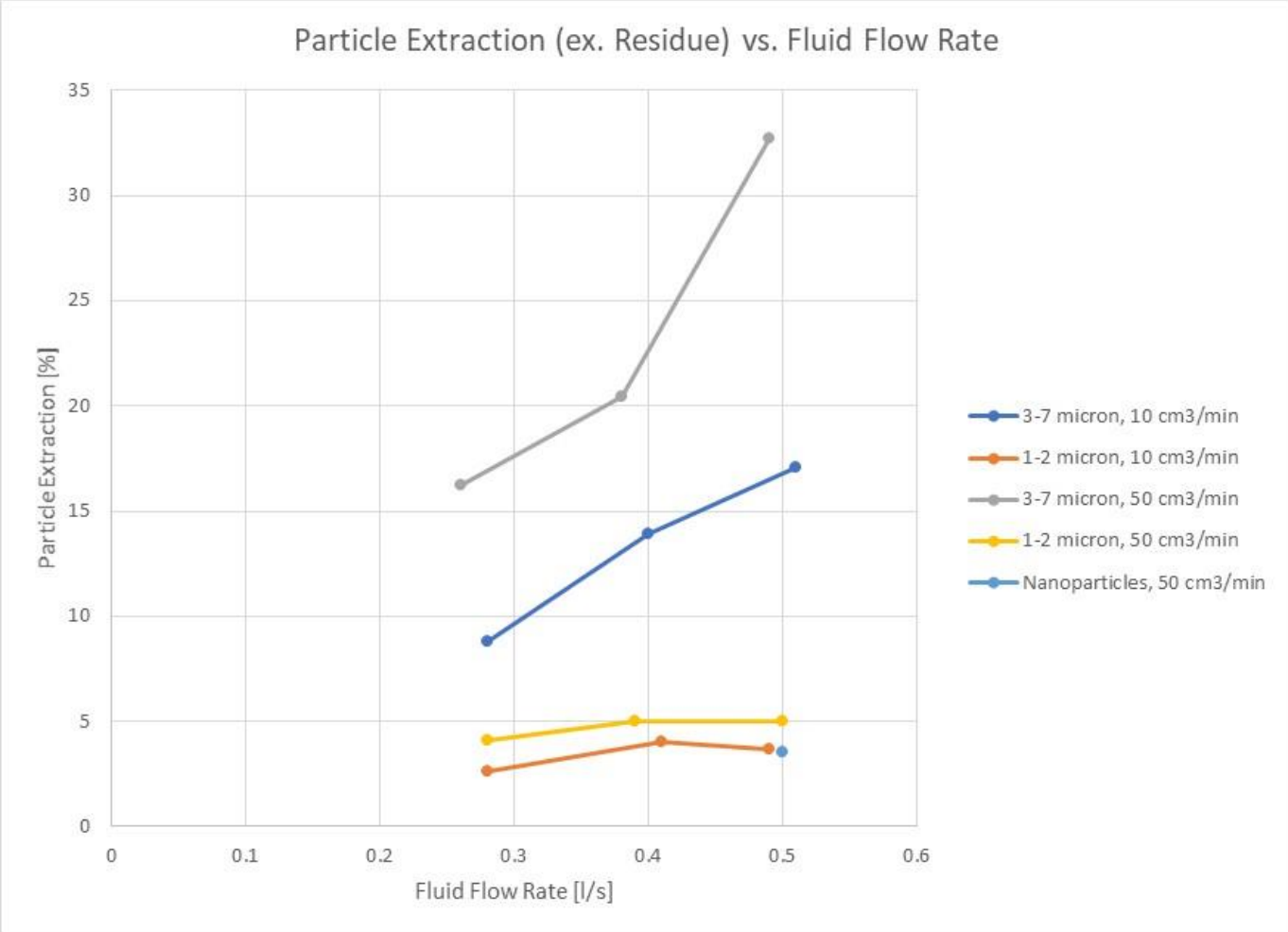

Figure 16. Particle extraction without including the residue sample per experiments plotted against the fluid flow rate.

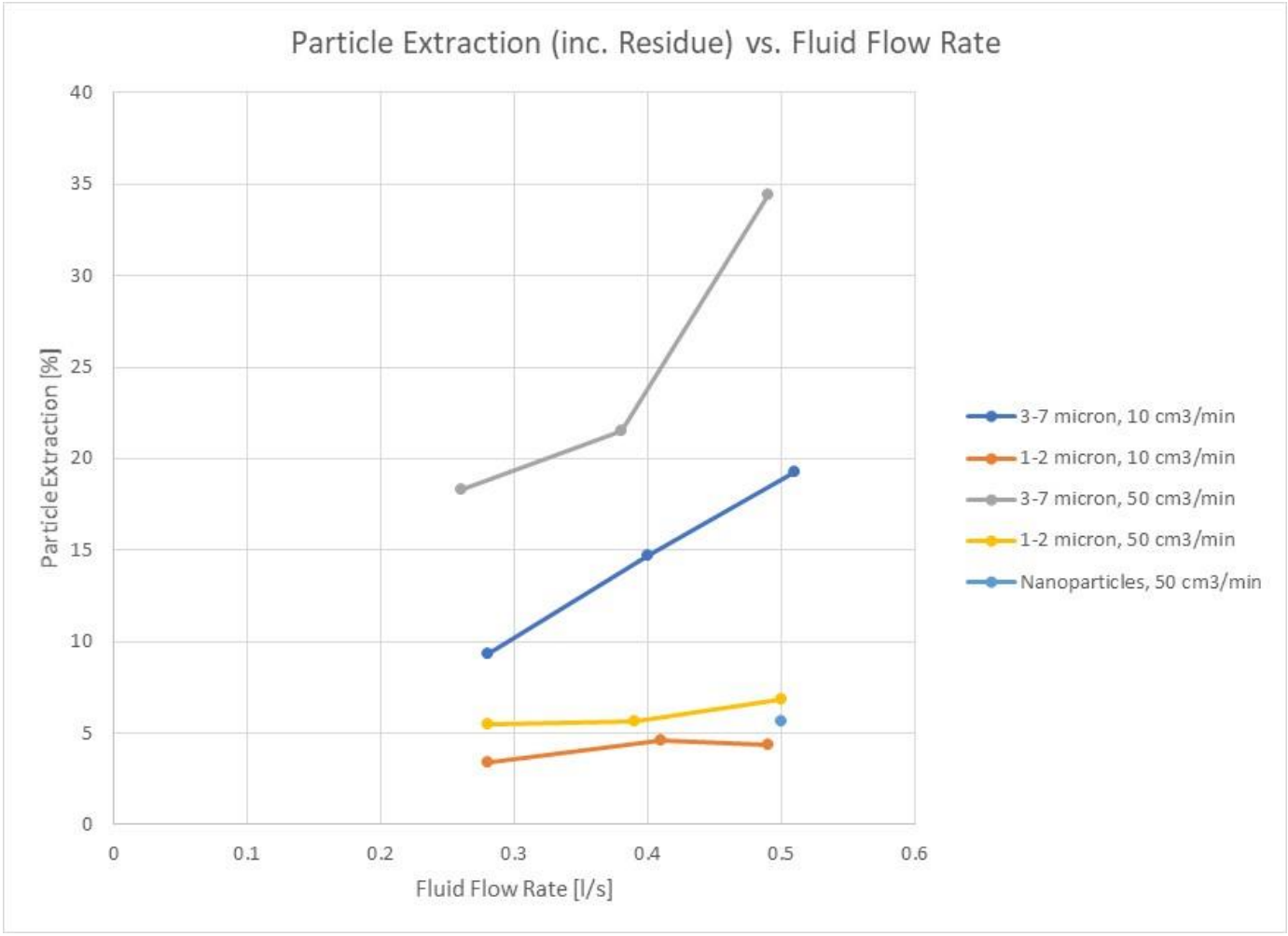

Figure 17. Particle extraction including the residue sample per experiments plotted against the fluid flow rate.

5. Discussion

5.1 Mean Bubble Size Measurements

Empirical data from the bubble size measurements, as depicted in section 4.1, suggests that the gas flow rate only has a marginal effect on the Sauter mean diameter of the bubble distribution. Noting that the formation of gas bubbles only occurs after gas has been injected, through the effect of fluid turbulence in the diffuser cone, the results could be deemed in agreement with the theoretical predictions made in section 3.1.2. In contrast, an increase in the fluid flow rate is seen to have an inverse effect on the Sauter mean diameter. In particular, at flow rates below 0.26 l/s, this inverse correlation appears to be most significant. The change in fluid flow rate dependency after 0.26 l/s could be correlated to the influences of other experimental setup elements on the mean bubble size, as a significant number of bubbles have been observed to circulate through the entire setup. In particular, the pump and the valves could possibly induce enough turbulence to be able to influence the coalescence and the breaking up of bubbles, thereby changing the mean bubble diameter.

It is important to mention that the uncertainty of the bubble size detected using the photographic method increases for high flow rates. Firstly, one of the most important steps in the processing and analysis stage of the images is the application of a threshold. For the threshold to apply optimally, as to make ellipse fit function optimally, bubble contours need to be distinct enough. However, at larger flow rates for either the gas flow rate or the fluid flow rate, images become increasingly more blurred and packed with bubbles. Based on which threshold values were used and what commands were used afterwards, one can observe the following errors (Figure 18):

1. contours of bubbles do not fully close and are thus seen as a ring formation of smaller bubbles,
2. the merging of adjacent bubbles due to blooming of the mask through the use of dilate and close--commands,
3. almost completely overlapping bubbles being recognized as a single large bubble.

Furthermore, as image details decline due to either a high gas flow rate or fluid flow rate, the bubbles become increasingly more difficult to distinguish and the uncertainty increases (Figure 19).

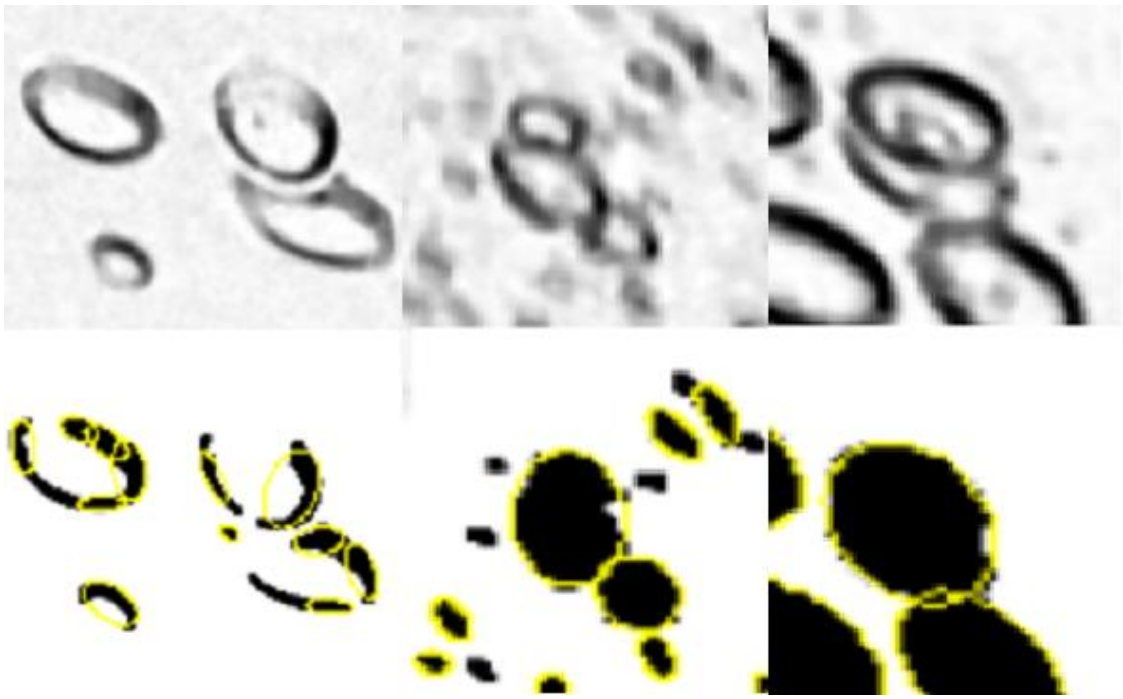

Figure 18. Examples of some of the analysis errors observed. From left to right: contours not closing, adjacent bubbles merging and overlapping bubbles.

Figure 19. Example images of bubbles for three different fluid flow rates at a fixed gas flow rate of 10 cm^3/min. From left to right: 0.14 l/s, 0.35 l/s and 0.58 l/s.

5.2 Mean Gas Holdup Measurements

The gas holdup measurement results as described in section 4.3, show a nearly linear correlation between the gas holdup volume and the gas flow rate. While there may be some experimental error resulting from measurement errors when evaluating the interface heights, the relative error compared to the increase in interface height can be assumed to be marginal, as the increase in interface height observed is typically close to half the length of the entire observation area. Since the mean bubble size has been observed to only change marginally with the gas flow rate, results can be said to be in agreement with earlier observations made by Massinaei et al. (Massinaei, et al., 2009), who reportedly observed a linear relation between the gas holdup and the bubble surface area flux. Consequently, the gas holdup measurements together with the bubble size measurements could be used to determine the total bubble interface area and the flow regime of the experimental setup. Both of which, may be used to determine the extraction efficiency for a given particle size.

5.3 Fine Particle Extraction Measurements

Looking at section 4.2.1, one can observe the time dependent curve for the fine particle extraction efficiency of all experiments, most of which can be described as growth functions with asymptotic behaviour. Only two curves show a slightly different trend: the "3-7 micron, 0.26 l/s, 50 cm^3/min" experiment and the nanoparticle experiment. While the reason for these discrepancies is not directly clear, some speculation can be had on the latter case. The difficulty of separating nanoparticles from the water-glycerol mixture due to their low sedimentation rate may be the cause of a higher experimental error compared to the other experiments.

Although the number of experiments with regards to different gas flow rates is low, the results in section 4.2.2 suggests that fine particle extraction is increased by increasing the gas flow rate as long as a homogeneous flow regime may be assumed. Additionally, an increase in fluid flow rate is generally also positively correlated with fine particle extraction efficiency. In particular, fluid flow rate appears to be of significant influence on the extraction of 3-7 micron sized particles, even more so than the gas flow rate. Furthermore, the data also suggests that a further increase in fluid flow rate may even be used to increase the total extraction even higher. In contrast, the highest flow rates of the 1-2 micron particle experiments suggest that an increase in fluid flow rate only correlates with an increase in fine particle extraction efficiency up until a certain fluid flow rate, which in this case appears to be near the highest fluid flow rates used. Thus, theoretically speaking, the highest fluid flow rates for the 1-2 micron sized particle experiments should roughly coincide with the optimal bubble size for the extraction of 1-2 micron sized particles. Based on the extraction data, the nanoparticle experiment was chosen to be performed for both the highest used gas flow rate and fluid flow rate.

Residue samples appear to indicate a relatively similar residue particle extraction for each experiment performed. Possibly leading to the conclusion that the residue particle extraction is mostly dependent on the setup and the used experimental method. Variations in the data could be explained by slight variations in the: gas-fluid interface height, and the methods used to take the residue sample and the preceding sample.

The observation of marginal changes in the gas-fluid interface height during the experiments leads to the conclusion that the change in bubble concentration or gas holdup is negligible. Combined with the particle extraction data of the 3-7 micron experiments, the appearance of a further decline in mean bubble size for higher fluid flow rates is formed. As the bubble surface area flux, a parameter that correlates to the particle extraction efficiency, is influenced by both the gas holdup and the mean bubble size.

The effect of particle size on the extraction efficiency observed during the experiments can be seen in section 4.2.2. When evaluating the recoveries under similar flotation parameters, a decline in extraction efficiency can be observed for a decrease in particle size. Theoretically speaking, the decline in particle extraction efficiency could be due to the decrease in bubble-particle collision (table 2).

Finally, a relatively low extraction efficiency of the nanoparticles could be ascribed to a low bubble-particle collision probability. As they have low inertia and therefore follow the streamlines around the bubble closely. Consequently, collision occurs only by Brownian motion.

6. Conclusion

In this study, relevant flotation parameters of fine particle flotation have been investigated and evaluated in an experimental setup to simulate a helium bubbling system designed for use in molten salt reactors. To this end, molybdenum particles of varying sizes and a water-glycerol (66-33 vol%) mixture were used to simulate the flow characteristic of a single-region molten salt reactor.

Analysis of bubble images for various gas flow rates and fluid flow rates has shown that the Sauter mean diameter of the bubbles produced by a Venturi type bubble generator remains relatively uninfluenced by the gas flow rate, while an increase in fluid flow rate decreases the Sauter mean diameter of the bubbles. Furthermore, mean gas holdup measurements have shown that an increase in the gas flow rate correlates to a linear increase in the observed gas holdup volume, which is in agreement with observations made by other researchers.

Fine particle extraction measurements have been performed and have shown that the effect of fluid flow rate plays a significant role in the total extraction observed, especially for 3-7 micron sized particles, where a further increase in fluid flow rate can still be used to increase the extraction efficiency even further. As the influence of the fluid flow rate appears to be significant, an increase in gas flow rate has also been observed to notably increase the extraction efficiency of every experiment. Furthermore, a decrease in particle size has been observed to correlate to a decline in fine particle extraction under similar experimental setup flow rates. Finally, a nanoparticle experiment was performed at a gas flow rate of 50 cm^3/min and a fluid flow rate of 0.50 l/s. The total extraction efficiency observed for the nanoparticles was 5.63%.

6.1 Recommendations

- A more extensive study where the influence of flotation parameters on fine particle extraction is investigated for a wider range of parameter combinations and where multiple experiments are performed per combination to increase the confidence level of the results.
- Other bubble size measurement techniques could be employed to increase the confidence level of the bubble size measurements. Alternatively, optimization of the image post processing and analysis stage and enhancement of the images themselves may lead to better results.
- During the experiments, vortices have been observed to form at the flotation column inlet and a significant number of bubbles have been observed to circulate the setup. Increasing the diameter of the column may increase the fraction of bubbles that escape the setup fluid current by reducing the turbulence observed at the inlet and could thereby also influence the flotation rate.
- Improvement of the recovery section in order to reduce the deposition on the Hallimond tube.
- The development of an intuitive fine particle flotation model, that has significant predictive power, may raise incentives to stimulate further flotation research in real reactors.

Bibliography

Campbell, J., n.d. *Molten Salt Reactor (MSR).* s.l.:Idaho National Laboratory.

Capelli, E. et al., n.d. *Noble metal behaviour and extraction in molten salt reactor,* s.l.: s.n.

Carter, W. L., 1968. *Decay Heat Generation by Fission Products and 233Pa in a Single-Region Molten Salt Reactor,* Oak Ridge: Oak Ridge National Laboratory.

Cheng, N. S., 2008. Formula for the Viscosity of a Glycerol−Water Mixture. *Ind. Eng. Chem. Res.,* 47(9), p. 3285–3288.

Furukawa, K., Alfred, L., Kato, Y. & Mitachi, K., 1990. Thorium Molten-Salt Nuclear Energy Synergetics. *Journal of Nuclear Science and Technology,* 27(12), pp. 1157-1178.

Gabbard, C. H., 1972. *Development of a Venture Type Bubble Generator for use in the Molten-Salt Reactor Xenon Removal System,* Oak Ridge: Oak Ridge National Laboratory.

Generation IV International Forum, 2018. *Gen IV International Forum.* [Online]
Available at: https://www.gen-4.org/gif/jcms/c_9260/public
[Accessed January 2019].

International Atomic Energy Agency , 2018. *Nuclear Power Reactors in the World,* Vienna: International Atomic Energy Agency .

International Energy Agency; Nuclear Energy Agency, 2015. *Technology Roadmap.* [Online]
Available at: https://www.oecd-nea.org/pub/techroadmap/techroadmap-2015.pdf
[Accessed January 2019].

Kaplan, P., 2008. *Developing countries eye nuclear power: report,* s.l.: Reuters.

Kedl, R., 1972. *The Migration of a Class of Fission Product (Noble Metals) in the Molten-Salt Reactor Experiment,* Oak Ridge: Oak Ridge National Laboratory.

Kowalczuk, P. B. & Drzymala, J., 2016. Physical meaning of the Sauter mean diameter of spherical particulate matter. *Particulate Science and Technology,* 34(6), pp. 645-647.

MacPherson, H., 1985. The Molten Salt Reactor Adventure. *Nuclear Science and Engineering,* Volume 90, pp. 374-380.

Massinaei, M. et al., 2009. Hydrodynamic and kinetic characterization of industrial columns in rougher circuit. *Minerals Engineering,* 22(4), pp. 357-365.

Nuclear Energy Advisory Committee; Generation IV International Forum, 2002. *A Technology Roadmap for Generation IV Nuclear Energy Systems.* [Online]
Available at: https://www.gen-4.org/gif/upload/docs/application/pdf/2013-09/genivroadmap2002.pdf
[Accessed January 2019].

Nuclear Energy Agency; Generation IV International Forum, 2014. *Technology Roadmap Update for Generation IV Nuclear Energy Systems.* [Online]
Available at: https://www.gen-4.org/gif/upload/docs/application/pdf/2014-03/gif-tru2014.pdf
[Accessed January 2019].

Orayeva, J., 2018. *Financing and Managing Nuclear Risks: The UK Model.* [Online]
Available at: https://www.iaea.org/newscenter/news/financing-and-managing-nuclear-energy-risks-the-uk-model
[Accessed January 2019].

Prakash, R., Majumder, S. K. & Singh, A., 2018. Flotation technique: Its mechanisms and design parameters. *Chemical Engineering & Processing: Process Intensification,* Volume 127, pp. 249-270.

Rosenthal, M., Kasten, P. & Briggs, R., 1969. *Molten-Salt Reactors - History, Status and Potential.* [Online]
Available at: http://moltensalt.org/references/static/downloads/pdf/NAT_MSRintro.pdf
[Accessed January 2019].

Schulze, H. J., 1984. *Physico-chemical Elementary Processes on Flotation.* Amsterdam-Oxford-New York-Tokyo: Elsevier.

Serp, J. et al., 2014. The molten-salt reactor (MSR) in generation IV: Overview and perspectives. *Progress in Nuclear Energy,* Volume 77, pp. 308-319.
Uhlır, J., 2007. Chemistry and technology of Molte Salt Reactors - history and perspectives. *Journal of Nuclear Materials,* Volume 360, pp. 6-11.
Yoon, R., 1993. Microbubble Flotation. *Minerals Engineering,* 6(6), pp. 619-630.
Yoon, R. & Luttrell, G., 1989. The Effect of Bubble Size on Fine Particle Flotation. *Mineral Processsing and Extractive Metallurgy Review,* Volume 5, pp. 101-122.
Yoon, R. & Mao, L., 1997. Predicting flotation rates using a rate equation derived from first principles. *International Journal of Mineral Processing,* Volume 51, pp. 171-181.

Appendix A: General ImageJ Script

```
//setTool("line");
makeLine(2532, 318, 2532, 3516);
run("Set Scale...", "known=26 unit=unit");
//setTool("rectangle");
makeRectangle(6, 474, 5550, 2904);
run("Crop");
run("8-bit");
run("Subtract Background...", "rolling=15 light");
run("Median...", "radius=5");
run("Enhance Contrast...", "saturated=0.4");
run("Duplicate...","title=QCheck");
//run("Threshold...");
setAutoThreshold("Otsu");
setOption("BlackBackground", false);
run("Convert to Mask");
run("Erode");
run("Open");
run("Close-");
run("Fill Holes");
run("Dilate");
run("Close-");
run("Fill Holes");
run("Dilate");
run("Dilate");
run("Fill Holes");
run("Erode");
run("Erode");
run("Ellipse Split", "binary=[Use standard watershed] add_to_manager add_to_results_table
merge_when_relativ_overlap_larger_than_threshold overlap=40 major=16-200 minor=16-200 aspect=1-
3.5");
run("Summarize");
```